Physica C 475 (2012) 60–68

Contents lists available at ScienceDirect

Physica C

journal homepage: www.elsevier.com/locate/physc

Study of junction and bias parameters in readout of phase qubits

Hesam Zandi [a,*], Shabnam Safaei [b], Sina Khorasani [a], Mehdi Fardmanesh [a]

[a] School of Electrical Engineering, Sharif University of Technology, P.O. Box 11365-9363, Tehran, Iran
[b] Department of Physics, Faculty of Sciences, Bilkent University, 08600 Ankara, Turkey

ARTICLE INFO

Article history:
Received 31 December 2010
Received in revised form 5 April 2011
Accepted 3 May 2011
Available online 10 May 2011

Keywords:
Phase qubit
Josephson junction
Tunneling
Quantum information

ABSTRACT

The exact numerical solution of the nonlinear Ginzburg–Landau equation for Josephson junctions is obtained, from which the precise nontrivial current density and effective potential of the Josephson junctions are found. Based on the resulting potential well, the tunneling probabilities of the associated bound states are computed which are in complete agreement with the reported experimental data. The effects of junction and bias parameters such as thickness of the insulating barrier, cross sectional area, bias current, and magnetic field are fully investigated using a successive perturbation approach. We define and compute figures of merit for achieving optimal operation of phase qubits and measurements of the corresponding states. Particularly, it is found that Josephson junctions with thicker barriers yield better performance in measurements of phase qubits. The variations of characteristic parameters such as life time of the states due to the above considered parameters are also studied and discussed to obtain the appropriate configuration setup.

1. Introduction

During last decade many efforts have been made in order to theoretically introduce and experimentally realize devices to be used as fundamental elements of a quantum computer [1]. Quantum bits (qubits) and quantum gates, so far, have been implemented in different physical systems including trapped ions [2,3], neutral atoms [4], optical systems [5,6] and superconductors [7–11]. Among all different types of qubits, those made of superconducting materials [12–14] are very promising and have attracted the attention of researchers, since they are easily scalable and their large electromagnetic cross section makes the coupling between them easy to achieve. Some recent experiments have successfully performed single- and multi-qubit gates [9,10]. Furthermore, a novel experiment reported successful fabrication and operation of a quantum information processor based on the superconducting platform [11]. In general, superconducting qubits can be classified into three main groups known as charge qubits, phase qubits, and flux qubits. Recently, the design developments of the circuit of a single-junction phase qubit [15] and optimization of the modulation of microwave pulses [16–20] have made the performance of high fidelity quantum gates possible. Other types of phase qubits are also introduced [21–23], but there is still considerable ongoing research on the single-junction phase qubits.

The main part of this device consists of a Josephson junction biased by a dc current. The potential energy of this system has the shape of a tilted washboard potential, and the two lowest eigenstates of the Hamiltonian are used as computational states $|0\rangle$ and $|1\rangle$. This is while higher energy levels might be present inside the potential well. The transition between these states in practice is done by applying modulated microwave pulses with frequencies in resonance with the transition frequency of the states $|0\rangle$ and $|1\rangle$. To measure the state of the qubit, a strong dc pulse lowers the barrier of the potential and increases the tunneling probability of the state $|1\rangle$. Therefore if the system is in this state, applying the measurement pulse leads to a change in superconducting phase across the junction, which consequently produces a voltage difference between two sides of the junction. Detecting this voltage drop allows us to measure the state of the qubit.

In a novel report, it has been shown that the straightforward quantum-limited measurement of mechanical resonators coupled to a phase qubit is possible [24], which asserts further importance of the measurement also in other applications. Working with high fidelity quantum computing system, one needs to know the precise tunneling probabilities of the states in order to analyze the measurement process.

One source of error in single-junction phase qubits can be attributed to the reduced fidelity of measurement for final states. In other words, the fidelity of measurement for states $|0\rangle$ and $|1\rangle$, after applying the measurement pulse, is not unity [7,14]. In this work, we address this problem by investigating the effects of several parameters such as the thickness of the insulating barrier of the junction, the size of cross section area, and the bias current on the tunneling rate of states $|0\rangle$ and $|1\rangle$, as well as externally applied magnetic field.

* Corresponding author. Tel.: +98 21 6616 5990.
E-mail address: zandi@ee.sharif.edu (H. Zandi).

0921-4534/$ - see front matter © 2011 Published by Elsevier B.V.
doi:10.1016/j.physc.2011.05.002

Nearly all of the existing studies on the phase qubits consider the Josephson current to be purely sinusoidal, which is a result of ignoring nonlinear terms in the governing differential equations (for example see Chapter 4 of [25]). This assumption is accurate enough if the thickness of the barrier is much smaller than the characteristic length of the superconducting material. However, to be able to work with junctions with thicker barriers, one needs to take into account all nonlinear terms in the Josephson junction dynamics. In this case the differential equation is not analytically solvable and a numerical approach is needed.

One of the most important parameters of any Josephson junction is the maximum super-current density known as the critical current density (J_c), which is calculated for both one (bulk) and two (thin-film) dimensional junctions [26]. In a relevant report, the super-current carrying density of states in diffusive mesoscopic Josephson weak links is calculated [27]. Including the geometry of the structure, different energy scales, and the nonidealities at the interfaces, the experimental results have been accurately described by the quasiclassical Green's-function technique in the Keldysh formalism. A comprehensive review by Golobuv et al. [28] discusses a wide range of Josephson junctions and their current-phase relation (CPR) by a quasiclassical approach.

"Silent" phase qubits containing Josephson junctions with nonsinusoidal CPR in a DC-SQUID are introduced and the effects of the ratio of the second harmonic amplitude to the first harmonic amplitude in CPR of YBCO junctions are discussed [29]. It is shown that a double-well potential with energy level splitting are the results of the higher harmonics of the impure CPR.

In another report, a mesoscopic qubit, made by d-Wave High T_c superconductors is proposed [30]. The physical concepts of time-reversal violation on surfaces and interfaces of these kinds of superconductors are used to break the conventional CPR in SND and DND junctions.

More recently, the optimal duration of the sinusoidal readout pulse and the depth of the potential well, for having the minimum readout error in the measurement process, are introduced in the frame of one-dimensional time dependant Schrödinger equation [20], corresponding to the conventional solutions of the Ginzburg–Landau equation excluding the nonlinear term.

Here, we present the results of numerical solution of complete Ginzburg–Landau equation and report the obtained super-current density and tunneling probabilities of eigenstates for several different cases. We compare our numerical results with an experimental data reported by Lucero et al. [7], which are found to be in very good agreement. We have also investigated the effects of various parameters, and depending on the particular application in the field of quantum information, we provide possibilities of obtaining a recipe for optimum design and readout procedure of phase qubits.

The paper has been organized as follows. In Section 2, after a brief introduction to the physics of single junction phase qubits (Section 2.1) and investigating the conventional Ginzburg–Landau equations in this respect (Section 2.2), we present a numerical precise solution of Ginzburg–Landau equation through a novel successive perturbation method (Section 2.3). We discuss the effects of junction and bias parameters, such as barrier thickness, and bias current (Section 3), on the tunneling rate of computational states, where we discuss how to obtain an optimum single junction phase qubit targeted for a better qubit setup in the circuit. Finally in Section 3.3 we investigate the effect of external magnetic field on the super-current density and consequently the tunneling rates. We conclude this work in Section 4.

2. Theoretical model

2.1. Principles of single junction phase qubits

Operation of phase qubits is connected to the eigenstates of the system defined in terms of the phase difference of a Josephson junction in a quantum circuit. In a superconductor, the current flows if and only if there is a phase difference in the wavefunction of the super-electrons over the position. In particular, the phase difference of the wavefunction across both sides of a Josephson junction δ, is strongly related to the current density through the differential equation obtained from the equation of motion [31]

$$\frac{\hbar}{2e}C\ddot{\delta}+\frac{\hbar^2}{2eR}\dot{\delta}+I_J=I_e, \tag{1}$$

where I_J is the induced current, I_e is the external current, C is the capacitance and $\mathcal{R}$ is the resistance of the Josephson junction. The above equation is based on the circuit description of the Josephson phenomenon. The potential function of this differential equation prescribes the specifications of the quantum system which is calculated and discussed in the following.

In Fig. 1, an example of the potential of a single Josephson junction is shown. The potential has a well with bound states, which according to the quantum theory opens up a probability of tunneling for any of these states through the barrier.

Suppose that with the aid of some external parameters, such as a bias current, the barrier is lowered. Evidently, the tunneling probabilities increase dominantly for higher states. If tunneling occurs for any of the given states, the change of the phase difference yields a voltage across the Josephson junction which can be read out. This phenomenon is the same for the first excited state if we increase the bias current further; this effect is used for measuring the state of the qubit. This added current is named "measurement current" and denoted by I_{meas}. Therefore the external current is a summation of the bias and measurement currents. The potential $U(\delta)$ is then computed from the current density $J(\delta)$, bias current I_b and the measurement current as follow:

$$U(\delta)=A\int J(\delta)d\delta-(I_b+I_{meas})\delta. \tag{2}$$

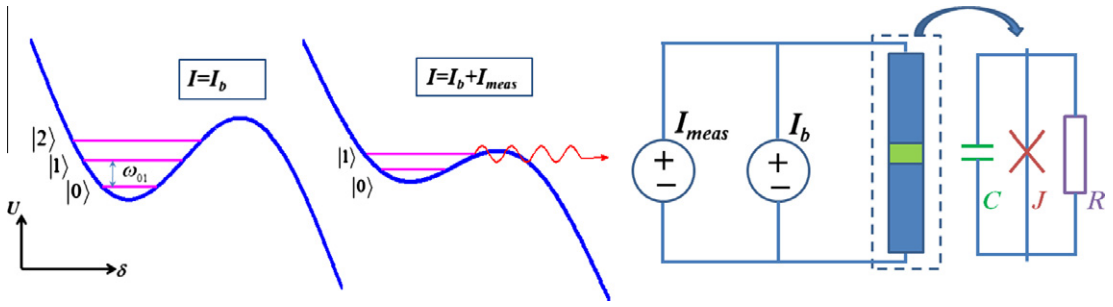

Fig. 1. Left: Potential energy of a biased phase qubit as a function of superconducting phase difference across the Josephson junction with respective bound states, before and after applying the measurement current. Right: The schematic circuit of a biased Josephson junction with applied measurement current.

2.2. Ginzburg–Landau equation based analysis

To obtain the accurate CPR $J(\delta)$, we analyze the Josephson junction in terms of the wavefunction of the superconductor through direct solution of the Ginzburg–Landau equation. As we shall observe in the next Section, experimental results can be accurately explained through this approach.

The Ginzburg–Landau equation is a phenomenological model of superconductivity, which yields the minimum energy state of the material, and reads [25]

$$\alpha\psi + \beta|\psi|^2\psi + \frac{1}{2m^*}\left(\frac{\hbar}{i}\nabla - \frac{e^*}{c}\mathbf{A}\right)^2\psi = 0, \tag{3}$$

where α and β are real-valued parameters depending on the superconductor material, and are respectively negative and positive. A numerical iterative approach for analyzing the two-dimensional system by minimizing the free energy is proposed earlier and the results in presence of the external magnetic field are reported [32].

We consider the structure to be effectively one-dimensional lying in an environment with no effective external fields. It is very common to define the normalized wavefunction as $f = \psi/\psi_\infty$, and the characteristic length of the superconductor as $\xi = \hbar\Big/\sqrt{2m^*|\alpha|}$, where $|\psi_\infty|^2 = -\alpha/\beta$ is the super-electron density at infinity. Hence, (3) takes the form

$$f - |f|^2 f + \xi^2\frac{d^2f}{dx^2} = 0. \tag{4}$$

The common practice in the solution of the above differential equation is to neglect the first two terms comparing to the third [25] and simply solve (4) as a linear 1-degree polynomial. After applying the boundary conditions $f(0) = 1$ and $f(L) = e^{i\delta}$, where L is the barrier thickness, the current density through the junction is found to be

$$J = \frac{e^*\hbar}{m^*L}|\psi_\infty|^2\sin(\delta). \tag{5}$$

We may improve the approximation by dropping only the second nonlinear term in (4). The answer of (4) would be a linear combination of two sinusoidal terms with appropriate coefficients satisfying the boundary conditions as:

$$f(x) = \frac{e^{i\delta} - \cos(L/\xi)}{\sin(L/\xi)}\sin\left(\frac{x}{\xi}\right) + \cos\left(\frac{x}{\xi}\right). \tag{6}$$

Consequently the current density through the junction becomes:

$$J = \frac{1}{\mathrm{sinc}(L/\xi)}\frac{e^*\hbar}{m^*L}|\psi_\infty|^2\sin(\delta). \tag{7}$$

This shows that the more accurate current density (7) actually differs from (5) with a factor of $\mathrm{sinc}(L/\xi) = \sin(L/\xi)/(L/\xi)$. Hence, in the limit of $L \ll \xi$ both of them result in identical expressions.

2.3. Calculation of the exact current density

Here, we present an exact solution to (4), including all three terms, which leads to a strongly nonlinear complex differential equation. This equation admits simple analytical solutions under zero boundary condition at infinity $f(\pm\infty) = 0$, known as solitons. However, it is not integrable under the boundary conditions $f(0) = 1$ and $f(L) = e^{i\delta}$, which motivated us to develop a new perturbative algorithm to obtain the fully accurate solution.

The algorithm is based on starting from the linear equation and allowing the nonlinearity to increase gradually. Then the solution is iteratively let to converge to match the strength of nonlinearity. Therefore, we insert a dimensionless switch coefficient k into (4) as

$$f - k|f|^2 f + \xi^2\frac{d^2f}{dx^2} = 0. \tag{8}$$

The parameter k is initially set to 0, representing zero-nonlinearity, and increased to the fully-nonlinear state 1 in N steps.

Now, we define the function series $\{f_n\}$ corresponding to the coefficient $k = n\varepsilon$, where $\varepsilon = 1/N$ is the step length. Trivially, f_0 is given by (6), while f_N is the desired solution. For $n >$ we define the perturbation function δf_n given by

$$f_n = f_{n-1} + \delta f_{n-1}. \tag{9}$$

If the total number of steps N is large enough, then the perturbation functions δf will be small, and we may safely neglect the nonlinear terms δf^m with $m > 1$. The functions $\{f_n\}$ are assumed to satisfy

$$f_n - n\varepsilon|f_n|^2 f_n + \xi^2\frac{d^2f_n}{dx^2} = 0, \tag{10}$$

from which the governing differential equation for δf could be found by substituting fn from (9) and applying the perturbation. Therefore, we reach at the second-order linear differential equation for δf as

$$\begin{aligned}\delta f_{n-1} - \varepsilon|f_{n-1}|^2 f_{n-1} + \xi^2\frac{d^2\delta f_{n-1}}{dx^2} - n\varepsilon(2|f_{n-1}|^2\delta f_{n-1} + f_{n-1}^2\delta f_{n-1}^*)\\ + \left[f_{n-1} - (n-1)\varepsilon|f_{n-1}|^2 f_{n-1} + \xi^2\frac{d^2f_{n-1}}{dx^2}\right] \simeq 0\end{aligned} \tag{11}$$

But according to (10), the expression within the brackets is zero. The remaining non-vanishing terms of (11) are complex-valued, yet we can conquer this problem by separating the real and imaginary parts of equation and reach a set of coupled differential equations for the real and imaginary parts of the main variable.

For the sake of simplicity we drop the trivial index $n - 1$ in (11) and employ the indices r and i corresponding to real and imaginary parts, respectively. Hence, we arrive at

$$\delta f_r - \varepsilon|f|^2 f_r + \xi^2\frac{d^2\delta f_r}{dx^2} - n\varepsilon(2|f|^2\delta f_r + \mathrm{Re}\{f^2\}\delta f_r + \mathrm{Im}\{f^2\}\delta f_i) \simeq 0 \tag{12a}$$

$$\delta f_i - \varepsilon|f|^2 f_i + \xi^2\frac{d^2\delta f_i}{dx^2} - n\varepsilon(2|f|^2\delta f_i - \mathrm{Re}\{f^2\}\delta f_i + \mathrm{Im}\{f^2\}\delta f_r) \simeq 0 \tag{12b}$$

The boundary conditions for the perturbation function $\delta f = \delta f_r + i\delta f_i$ are quite simple; f_0 satisfies the boundary conditions $f(0) = 1$ and $f(L) = e^{i\delta}$. Therefore, the new boundary conditions for the perturbation functions are

$$\delta f_r(0) = \delta f_i(0) = 0, \tag{13a}$$

$$\delta f_r(L) = \delta f_i(L) = 0. \tag{13b}$$

By reinserting the answers in (12) and repeating the procedure until $k = 1$ (or $n = N$), we can find the final result for an arbitrary Josephson junction. The accuracy can be arbitrarily increased by increasing the number of steps N.

We can also include the effect of an externally applied magnetic field as mentioned in (3). In presence of the external magnetic field, the governing differential equation becomes

$$\left(\alpha + \frac{e^{*2}|\mathbf{A}|^2}{2m^*c^2}\right)\psi + \beta|\psi|^2\psi + \frac{ihe^*A_x}{m^*c}\frac{d\psi}{dx} - \frac{\hbar^2}{2m^*}\frac{d^2\psi}{dx^2} = 0. \tag{14}$$

In case of an external magnetic field with parallel vector potential to the surface of the junction ($A_x = 0$), and after normalization we have

$$f - \frac{1}{1-\chi|\mathbf{A}|^2}|f|^2 f - \frac{\hbar^2}{2m^*\alpha(1-\chi|\mathbf{A}|^2)}\frac{d^2 f}{dx^2} = 0. \quad (15)$$

where $\chi = -e^{*2}/2m^*c^2\alpha$. Since α is negative, the material stays in the superconducting state as long as the effective characteristic length defined by

$$\xi_{eff} = \frac{\hbar}{\sqrt{2m^*|\alpha|(1-\chi|\mathbf{A}|^2)}}. \quad (16)$$

remains finite.

3. Results and discussion

Based on the above resolution, the results of the calculated parameters needed for reaching to the optimal operation of the phase qubit are analyzed and explained as follow:

3.1. Current density

In this section, we present the exact current density computed numerically from the set of coupled differential Eqs. (12). We scale all position parameters by the characteristic length ξ.

As it can be seen in Fig. 2, the exact current density is non-sinusoidal and is antisymmetric, in the sense that $J[(n+\frac{1}{2})\pi+\delta] \neq J[(n+\frac{1}{2})\pi-\delta]$. Rather than that, it seems that higher odd harmonics appear in the exact solution of CPR which makes it highly unfamiliar compared to the conventional solutions. As for deformations of the potential well constructed from the above solution, these transfigurations will affect the tunneling probabilities and theoretical predictions of qubit readout outcome which are the very subjects of this article. In Fig. 3 the relative differences of the exact and conventional (5) solutions are shown, for various thicknesses of the barrier. Obviously, the difference is small in the limit of $L \ll \xi$, but for larger values of L the difference ratio exceeds 10% which is quite significant.

3.2. Tunneling probability

After calculating the exact current density versus phase difference, we can find the resulting effective potential. Then, one may readily compute the eigenstates of the median well through (2). The cross section of the Josephson junction is taken to be $A/\xi^2 = 100$ everywhere, unless stated otherwise.

Obviously there are some bound states confined inside the well and unbounded states. The exact analytic form of the states

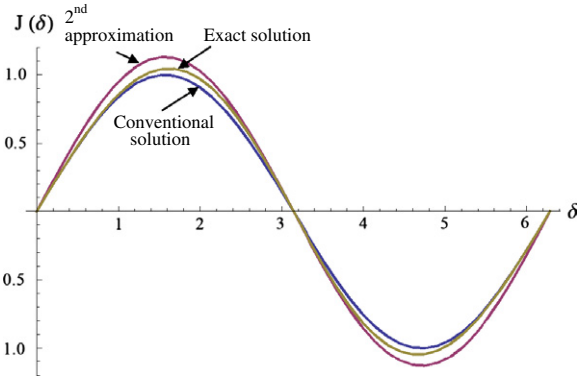

Fig. 2. Current densities obtained from the simplest conventional form of the differential Eq. (5), the 2nd approximation by including both linear parts (7), and the exact solution of full nonlinear differential Eqs. (12) versus the superconductive phase difference across the junctions for $L/\xi = 0.85$.

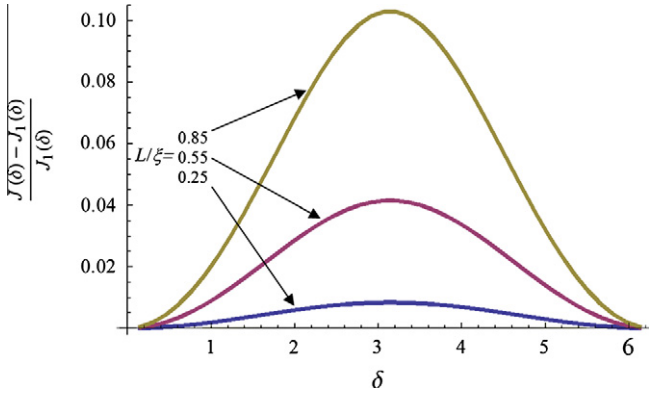

Fig. 3. Relative difference Ratio of the exact (J) and conventional (J_1) current densities for different barrier thicknesses $L/\xi = 0.85$, 0.55 and 0.25 versus the superconductive phase difference across the junction.

(energies) could not be found; therefore we use a perturbation theory and use a typical harmonic oscillator, which is fully studied, as the unperturbed potential. We fit the parabolic harmonic oscillator by assuming the same concavity at the minimum of the potential well. We also normalize the energy in our calculations to $E_c = 2e^2/C = 0.1$ and use second order perturbation for computing the energies of the first three states. These include the ground state $|0\rangle$, the first exited state $|1\rangle$ for defining the qubit, and the third state $|2\rangle$. Knowledge of the latter state allows the study of the leakage outside the qubit manifold.

Long-lived bound states and optimum measuring parameters require the appropriate ratio of the bias current and the critical current of the Josephson junction. Usually the first three states are designed to be bounded in the well constructed by the Josephson junction and the bias current, meanwhile higher states are unbounded. Increasing the bias current lowers the barrier potential and makes the third state unbounded, hence the tunneling rate of the third state through the barrier in this situation would be very high.

We assume that the measurement current is applied adiabatically so that the states also change accordingly. This is related to the time constant of the system over which system evolves to a new subspace. Therefore the ground and excited states gradually shift to match the new instantaneous condition.

For calculating the tunneling rates we discretized the phase interval in the stepwise manner, and employed the transfer matrix method [33]. The interval extends from the bottom of the well to the same potential point behind the barrier. This procedure is performed for each measurement current between zero and I_cI_b, which is the difference between the critical current of the junction and the bias current. Due to the perturbation we used for the calculation of states, it is not possible to perform this algorithm near the end point. Hence we considered two conditions: $E_B < E_0 < E_1 < E_2$, and $E_2E_1 < E_1E_0$ to prevent such miscalculation, where E_B is the energy at the bottom of the well. The above conditions are trivial results for a potential which has a larger concavity over its well. The second condition is equivalent to $\omega_{12} < \omega_{01}$ which means that the main transition frequency is larger than the second one. For the first three states of the well, these calculations are done and the results are shown in the next set of figures. Higher states have higher probability of tunneling with the same measurement currents. Henceforth, the sequence of the tunneling curves is always as the state number is increasing from right to left.

The experimental data of tunneling rates, extracted from [6], are shown in Fig. 4 (circles). The superconductor material used in the

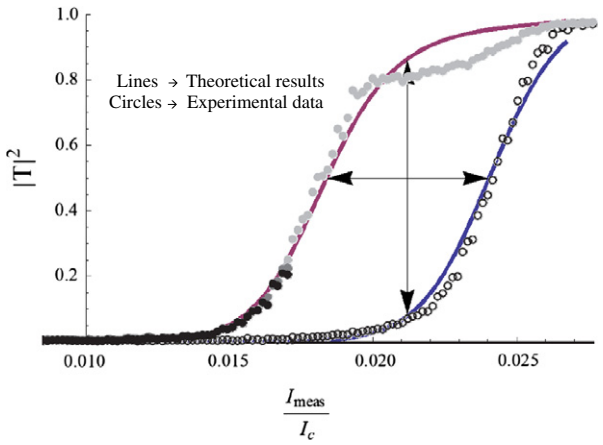

Fig. 4. Tunneling probabilities of the main qubit manifold states ($|0\rangle$ and $|1\rangle$) versus the normalized applied measurement current (I_{meas}/I_c). Circles: Experimental data extracted from Ref. [7] for barrier thickness of $L/\xi = 0.02$, and cross section of $A/\xi^2 = 100$. Solid lines: our numerical results for the same parameters with respect to the reported experimental data, and estimated bias current of $I_b/I_c = 0.97$ for best fitting.

experimental setup was supposed to be Al with an intrinsic coherent length of about 100 nm, tunnel barrier width of $\sim$ 2 nm, and junction cross section $A = 1\ \mu m^2$ [34]. The coherent length of Aluminum has been reported for bulks to be $\sim$1600 nm and much less for thin films in many articles [35–37]. Here thin film is considered for the qubits and we took an average of 100 nm based on the reported values [38–40]. Using these parameters, we calculated the tunneling rates and have shown them at the same plot (solid lines).The reason for deviation in larger measurement currents is that the calculation of the eigenenergies of the potential well is not accurate enough; under such circumstances, even the second-order perturbation theory fails to properly predict the exact states.

There are two figures of merit which we are focusing on: the fidelity of measurement F which is the maximum difference between the two tunneling rates corresponding to the ground and first excited states over the measurement current. This fidelity distinguishes the optimum current (I_{opt}) for measurement which is also critical for some applications. The second figure of merit is the ratio $\mathcal{R}$ of the difference between measurement currents at the 50% transmissivity of the first and second states with respect to the optimum current ($\Delta I/I_{opt}$). In Fig. 4, besides the qualitatively similar shapes, the figures of merit are in agreement with our numerical result.

It is evident that higher fidelity F (ideally unity) is the most important goal of this systematic approach, but there are other considerations which guide us through more details in qubit tunneling rates. For better understanding the reason for defining other figures of merit, it is instructive to consider any possible assumptions for the variation of these tunneling rates and discuss about each situation.

First of all considering a situation shown in Fig. 5a, the fidelity of measurement (F) is obviously unity but the difference between two measurement currents (ΔI) is very small so that the optimum current lies strictly in between. This is not a desired situation, where the fluctuations of the measurement current may lead to catastrophic behavior of the system. Hence even an utmost ideal fidelity is not sufficient to gain the best status, while larger differences between the two tunneling rates make the system much more reliable. In Fig. 5b two similar situations are shown with same measurement current differences (ΔI) but dissimilar optimum currents (I_{opt}). Dashed curves in the figure are related to the tunneling rates of the second excited state which is not in the qubit manifold but plays an important role in the characteristics of the qubit. For the black (dark) curve in the figure, which has higher optimum current, the tunneling probability of the second excited state is much lower than the green (light) curve which means that this unwanted state has longer life time, while the life time of the lower states does not change significantly. In general the existence of these unwanted states may lead to lose information or cross talk issues in a network of qubits. Hence the green (light) curve ensures better measurement results. One can propose a situation like Fig. 5c which is actually worse than the previous case, because rather than the issue of the second excited state, the fidelity F of the black (dark) curve is severely dropped. For the last example, two cases with the same optimum currents but dissimilar differences of the measurement currents are compared in Fig. 5d. It is shown from the first example that small ΔI is not favorable; here we can see it in a more like a real situation. Our choice would be the black (dark) curve which has higher ΔI, less suffers from the second excited state, beside having higher $\mathcal{F}$. The outcome of this argument is the reason for defining $\mathcal{R}$ as mentioned before, which means that higher differences in measurement currents (ΔI) and smaller optimum currents (I_{opt}) are desired simultaneously.

We compare the results of our numerical calculations with the conventional simple solution of the Josephson junction. The tunneling probabilities of the states are plotted in Fig. 6. As it can be seen, the first noticeable change of tunneling probabilities obtained from the exact potential (dark/blue lines) is shifting to the lower values of measurement currents. Therefore the optimum measurement current decreases about 25% from $I_{meas}/I_c = 0.276$ to $I_{meas}/I_c = 0.207$, when accurate results are used instead of (5). Moreover, $\mathcal{R}$ is increased about 33% from 0.507 to 0.676, meaning better noise immunity than what could be expected from the simple solution (5). At the same time, however, $\mathcal{F}$ is slightly decreased less than 1% which is negligible due to vast improvement of other parameters.

Although the thermal variations of the qubit environment are very effective and might overcome the discussing parameters, the temperature dependence of the qubit and its parameters is beyond the scope of this work; hence analogies between thermal effects and the discussed parameters in the article are not brought here.

3.2.1. Effects of the barrier thickness

Variations of the figures of merit and the optimum current of measurement with respect to the barrier thickness are shown in Fig. 7. We can see that $\mathcal{R}$ shows a noticeable growth in higher thicknesses; however $\mathcal{F}$ does not take effect significantly. This is while the optimum current I_{opt} desirably decreases slowly. The results are shown based on both, the conventional (red circles) and exact (blue squares) solutions of the Ginzburg–Landau equation.

The qualitative behavior of $\mathcal{R}$ and I_{opt} is the same, but it seems that the results of the new exact solution for F are in contrary to the conventional one. This behavior might rise from the fact that the Josephson Effect in high thicknesses of the barrier is much weaker and hence the coupling of the wavefunctions across the junction decreases. Therefore the effects of none intrinsic parts of the Ginzburg–Landau equation, override the situation.

From the exact solution in Fig. 7a, $\mathcal{F}$ is approximately 0.785 for $L/\xi = 0.25$ and occurs at $I_{opt} = I_{meas}/I_c = 0.062$. In contrast, for $L/\xi = 0.85$, $\mathcal{F}$ is approximately 0.782 and occurs at $I_{opt} = I_{meas}/I_c = 0.05$. We can see that $\mathcal{F}$ is slightly decreased about 0.4%, but willingly the value of the optimum measurement current also decrease by 20%. It should be noticed that I_c itself is smaller for wide Josephson junctions, that means one would need a much lower current for a reliable readout. This point is highly desired for

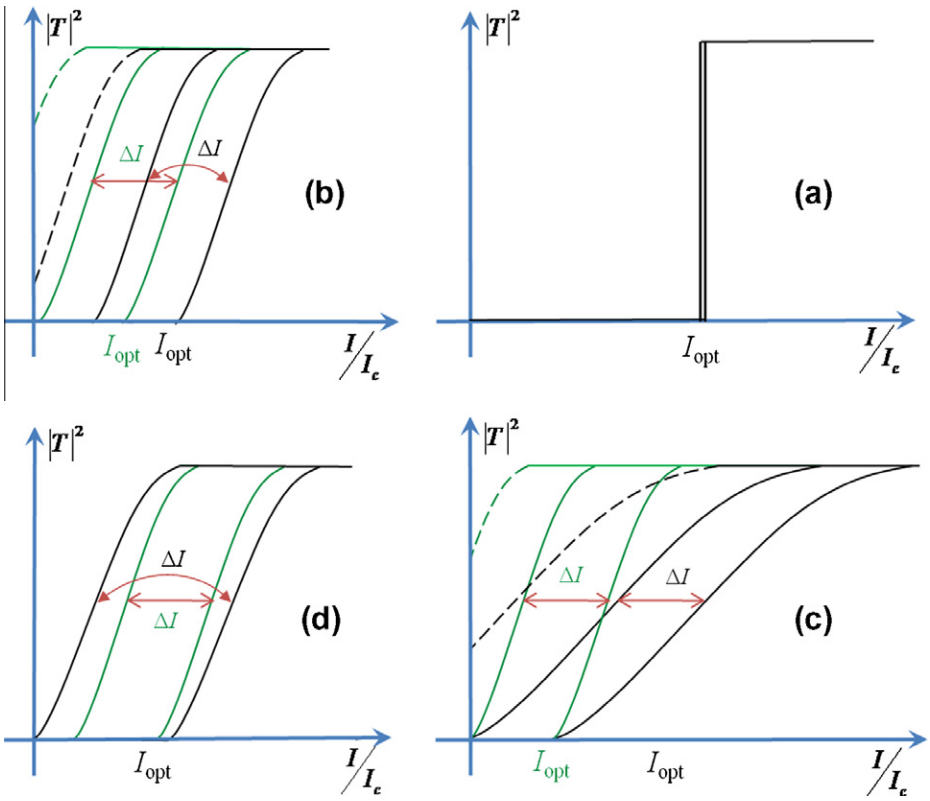

Fig. 5. Possible assumptions for tunneling rates of qubit states to explain the reason of defining the figure of merit $\mathcal{R}$. (a): Despite having a unity value for Fidelity ($\mathcal{F}$), this situation lacks the reliability of measurement according to the small interval of acceptable measurement currents. (b): considering tunneling rates having the same measurement current differences (ΔI), the green (light) one having lower optimum current is much more desirable in order to be much less affected by the second excited state having lower life time. (c): in this case, life time of the second excited state in the black (dark) curve is better than the previous case, but the fidelity ($\mathcal{F}$) is severely dropped, hence the green (light) curve is still favorable. (d): the black (dark) curve has higher fidelity (($\mathcal{F}$)) and less affected by the second excited state, because of having higher measurement current difference (ΔI), being a better choice. (For interpretation of the references to color in this figure legend, the reader is referred to the web version of this article.)

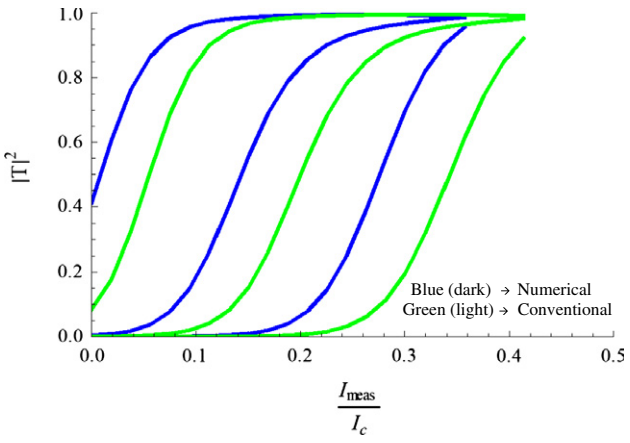

Fig. 6. Tunneling probabilities of first three states versus measurement current for $L/\xi = 0.85$ and $I_b/I_c = 0.5$; Blue (dark): exact numerical solution. Green (light): conventional approximation obtained by (5). (For interpretation of the references to color in this figure legend, the reader is referred to the web version of this article.)

reduction of the sensitivity to noise, and thereby better noise immunity. Now we turn to the next figure of merit $\mathcal{R}$ in Fig. 7b. For $L/\xi = 0.25$, $\mathcal{R}$ is approximately 0.27, while For $L/\xi = 0.85$ it increases to about 0.55. Larger $\mathcal{R}$ corresponds to better recognition of states, meaning less chance of error in readout. We hence notice that this figure of merit is improved by 103%.

3.2.2. Effects of the bias current

The main effect of the bias current is the ability to control the number of bound states in the constructed well potential. The qubit just needs two states to properly operate; hence, higher states are not desired and may have destructive effect on the operation of the qubit due to leakage. There exists a great deal of research conducted to reduce this chance [15,41].

We cannot completely get rid of leaking states, because we anyway need to keep some distance from $|1\rangle$ to the peak of the barrier to suppress the tunneling rate for stabilizing the first excited state $|1\rangle$ of the qubit. After all, there is a tradeoff between the existence of leakage states and the stability of the exited state $|1\rangle$ of the qubit. Since our work is not focused to study the leakage in qubits, we just investigate the effect of bias current in the tunneling probabilities of the qubit states.

For stabilizing the state $|1\rangle$ in qubit, we considered the constraint $|T|^2 \leqslant 0.001$ for the tunneling probability of this state with no measurement current, which leads to a maximum acceptable bias current. The figure of merit $\mathcal{F}$ almost does not change versus bias current; however, $\mathcal{R}$ increases significantly. On the other hand, the diagram has its maximum shift toward the origin and fortunately the value of optimum measurement current has its minimum value and $\mathcal{R}$ reaches its maximum value, implying superior noise immunity.

3.2.3. Effects of the cross section

The cross section of the Josephson junction strongly influences the critical current of the junction. The variations of the figures of merit ($\mathcal{F}$ and $\mathcal{R}$), optimum measurement current and the

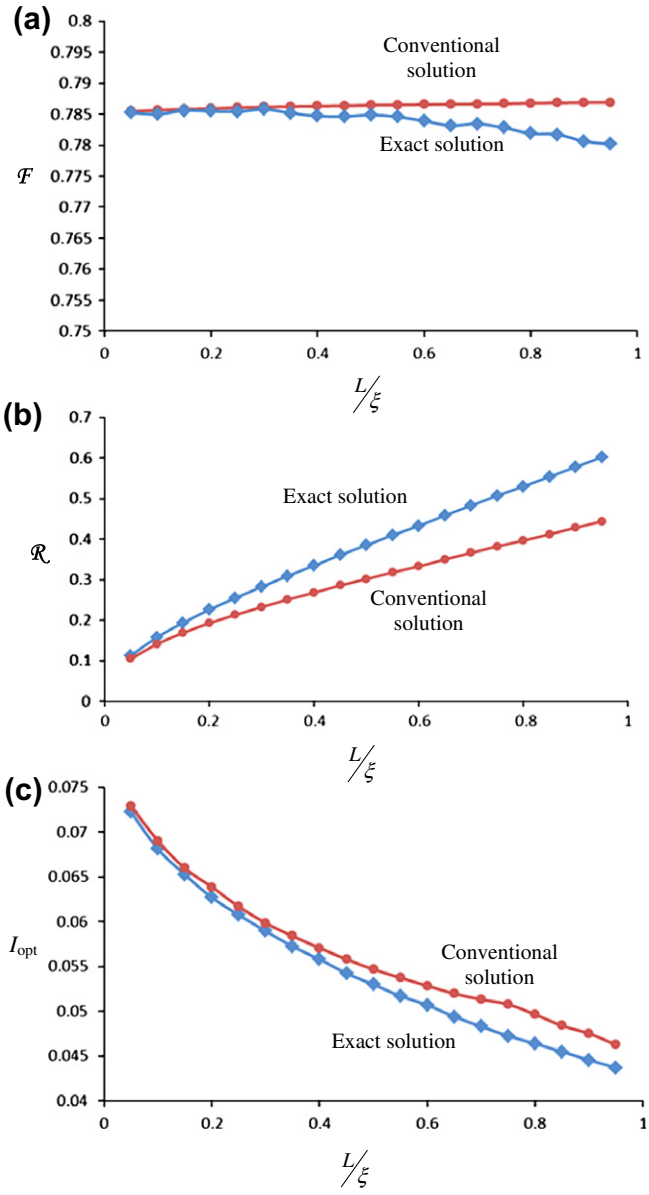

Fig. 7. Variations of the figures of merit ($\mathcal{F}$) and $\mathcal{R}$) and the optimum current of measurement (I_{opt}) versus the barrier thickness for $I_b/I_c = 0.915$. Red circles: results based on the conventional solution, and blue squares: results based on the exact solution of the Ginzburg–Landau equation. (For interpretation of the references to color in this figure legend, the reader is referred to the web version of this article.)

corrected bias current needed for setup versus the cross section of the junction for the width of $L/\xi = 0.85$ has been plotted in Fig. 8.

The qualitative behavior of the shown parameters, are the same, except for $\mathcal{F}$. It is shown in Fig. 8a that based on the exact solution (blue squares), $\mathcal{F}$ increases in contrary to the results based on the conventional solution (red circles). This behavior might again rise from the fact that the Josephson Effect in the lower cross sections is much weaker and hence the coupling of the wavefunctions across the junction decreases. Therefore the effects of none intrinsic parts of the Ginzburg–Landau equation, override the situation. Considering the curves based on the exact solution, the following results and discussions are presented.

The variations of $\mathcal{R}$, shown in Fig. 8b, are best fitted by a logarithmic function decreasing while the cross section increases, but this would be at the expense of slightly smaller $\mathcal{F}$. We have considered the life time condition for the state $|1\rangle$ discussed in previous

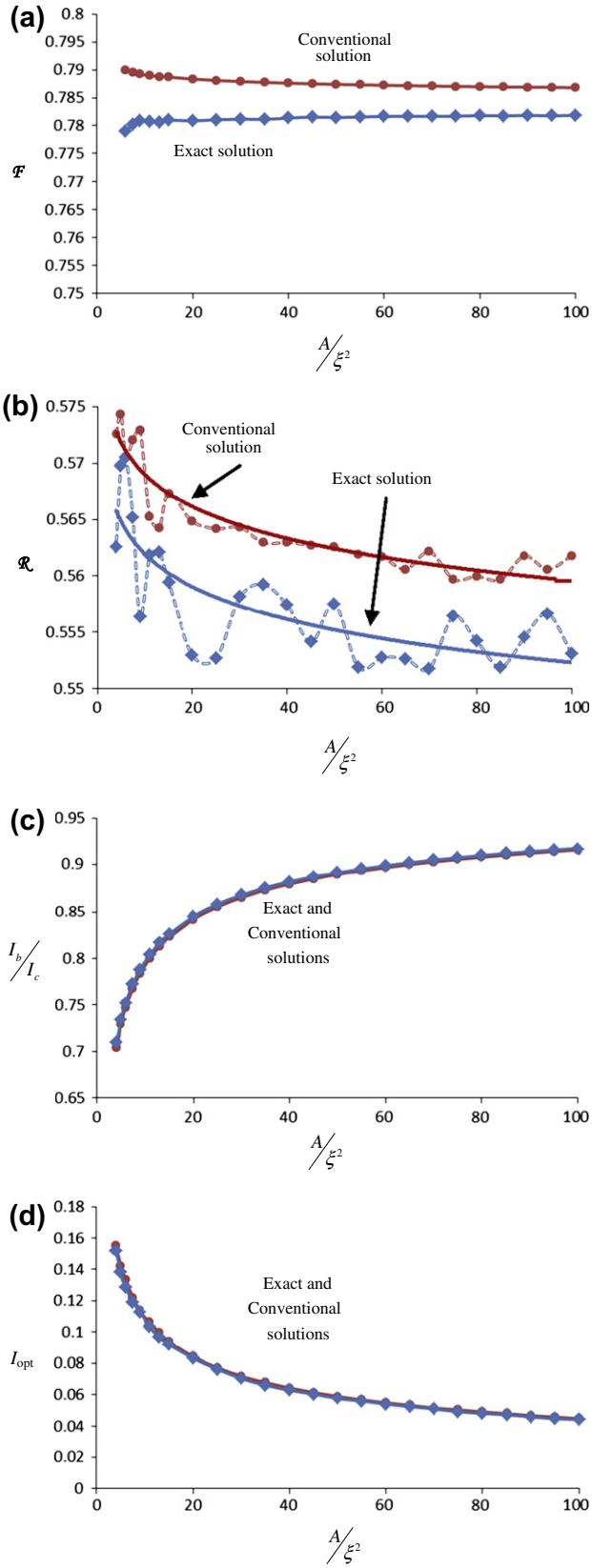

Fig. 8. Variations of the figures of merit ($\mathcal{F}$) and $\mathcal{R}$), optimum measurement current (I_{opt}), and the corrected bias current needed for better measurement versus the cross section of the junction for $L/\xi = 0.85$. The solid line in (b) is best fitted by a logarithmic curve. Red circles: results based on the conventional solution, and blue squares: results based on the exact solution of the Ginzburg–Landau equation. (For interpretation of the references to color in this figure legend, the reader is referred to the web version of this article.)

section by increasing and setting the bias current to the point satisfying $|T_1|^2 = 0.001$. The corrected values for the bias current are shown in Fig 8c, where shows that for higher cross sections, the needed current for having the same life time is saturated and the variations are not simply linear. The optimum measurement current I_{opt} is shown in Fig. 8d which rises significantly and all these variations are strengthened in lower cross sections. For some situations, smaller cross sections lead to better results, but this also has its own limits. In fact, extremely small cross sections cannot be properly realized in the fabrication process.

3.3. Effects of the external magnetic field

The magnetic field suppresses the wavefunction and deteriorates the superconductivity. However, we are looking for symmetry breaking effect of the magnetic field, in the current density of the Josephson junction versus phase difference as discussed earlier in the beginning of Section 3. The effective characteristic length defined in (16), always exceeds the intrinsic value under magnetic field. Therefore, the operation of junction moves toward smaller width, as the ratio L/ξ_{eff} decreases. At the same time, however, the nonlinearity strength according to (15), increases by the factor $(1 - x|A|^2)^{-1}$, hence the ultimate result could not be predicted easily. For the case of having a linear vector potential in the direction of the current through the junction, which is made by a constant magnetic field parallel to the surface of the junction, we can approximate the vector potential by a constant vector in the range of junction barrier length and calculate the CPR.

The effects of external magnetic field by the relative ratio of current densities are shown in Fig. 9 for weak ($x|A|^2 = 0.2$), medium ($x|A|^2 = 0.5$) and strong ($x|A|^2 = 0.83$) magnetic fields with $L/\xi = 0.85$. Considering the value of 100 nm for characteristic length of Aluminum and using the famous relation for the characteristic length of a superconductor with respect to the Ginzburg–Landau Coefficient α [25], we can find the respected values of the needed external magnetic fields for having the mentioned situations. Thus, the physical values for weak, medium and strong magnetic fields for the above situation would be about 1.7 mT, 4.2 mT and 7 mT respectively. It is observed that for medium values of magnetic fields, the antisymmetric behavior in current density is well pronounced and the nonlinearity is much stronger.

The Variations of the figures of merit ($\mathcal{F}$ and $\mathcal{R}$) and the optimum current of measurement for $L/\xi = 0.85$ and bias current of $I_b/I_c = 0.915$ for different amplitudes of the external magnetic field are shown in Fig. 10.

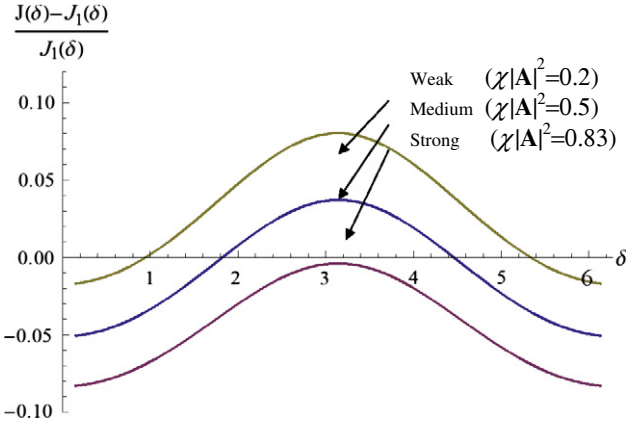

Fig. 9. Relative difference of the exact (J) and conventional (J_1) current densities in presence of an external magnetic field for a weak, medium and strong one with $L/\xi = 0.85$.

The probability of tunneling for the first exited state, when no measurement current is applied, increases less than one order of magnitude when the amplitude of the external magnetic field is increased. Therefore it seems that no bias current correction is needed. It is very interesting that the normal vector potential through the junction improves both figures of merit. The authors believe that this behavior is due to the interaction of cooper-pairs and the external magnetic field, which obviously shows itself in the effective characteristic length of the superconductor. It seems that applying the external magnetic field induces vortices of super-currents in the Josephson junction and improves the characteristics of the potential well in the phase qubit. According to the structure of the phase qubit, there are high sensitive devices in the circuit connected to the phase qubit which have large interactions with magnetic fields. Since this locally applied magnetic field affects only the Josephson junction, the above discussions still

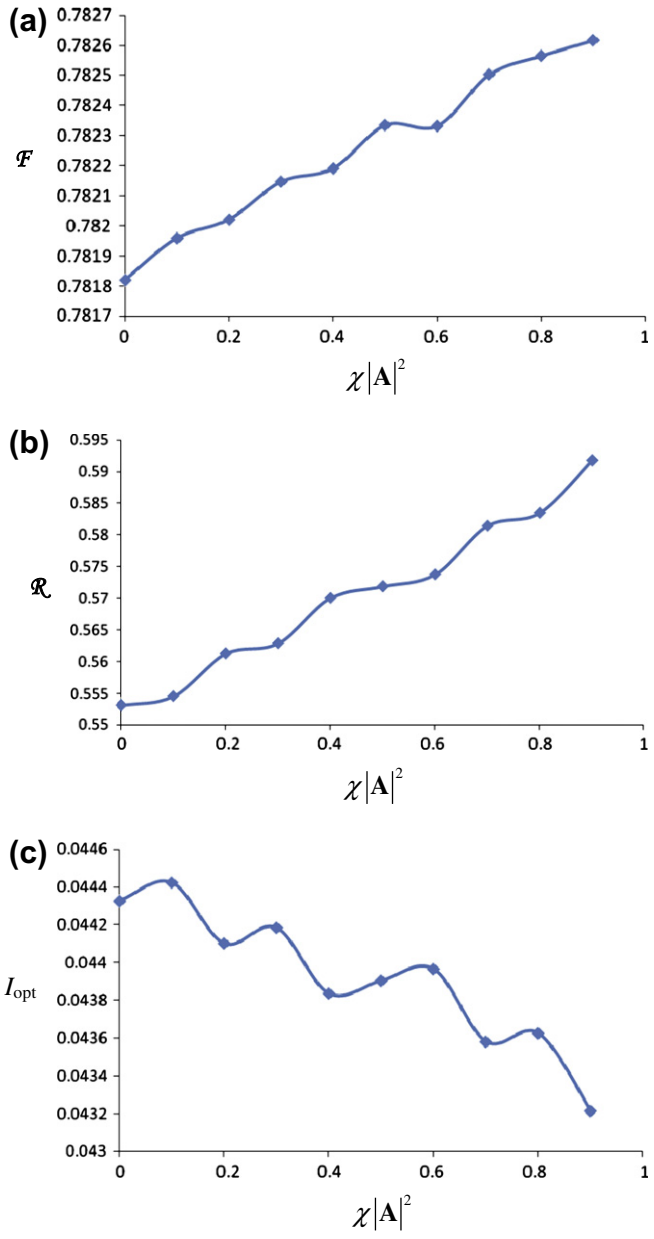

Fig. 10. Variations of the figures of merit ($\mathcal{F}$) and $\mathcal{R}$) and the optimum current of measurement (I_{opt}) with $L/\xi = 0.85$ and bias current of $I_b/I_c = 0.915$ versus the amplitude of the external magnetic field.

hold, otherwise any unwanted physical event caused by interaction of this external magnetic field with other parts of the qubit setup might weaken the characteristics of the qubit. Therefore an appropriate layout of the quantum circuit is desired to be designed in order to control all effects of this external magnetic field on the whole system.

4. Conclusion

We presented a comprehensive analysis of tunneling rates in Josephson junction phase qubits. For this purpose, we devised a successive perturbation approach to obtain the exact numerical solution of the Ginzburg–Landau equation. We defined two figures of merits for optimal readout of phase qubits, and investigated the effects of various internal and external parameters on them. We found that in general, larger thicknesses of the barrier and for some situations, smaller cross sections lead to better results, while at the same time they are subject to practical limits. We found the optimum value of the bias current by setting a constraint for the stability of the qubit considering that large bias currents dictate short-lived states, while small bias currents lead to chances of information loss. We furthermore observed that external magnetic field imposes strong CPR asymmetry, and it has positive effects on all figures of merit for the system. We also compared our numerical results with experimental data reported elsewhere and observed very good agreement.

Acknowledgment

The authors wish to thank Dr. Fabio Taddei at National Enterprise for nanoScience and nanoTechnology (NEST), Scuola Normale Superiore di Pisa (SNS), Italy, for careful reading of the manuscript and providing very valuable suggestions. This work was supported in part by the Research Deputy of Sharif University of Technology through graduate and postdoctoral scholarships provided respectively to H. Zandi and S. Safaei.

References

[1] T.D. Ladd, F. Jelezko, R. Laflamme, Y. Nakamura, C. Monroe, J.L. O'Brien, Nat. Rev. 464 (2010) 08812.
[2] C. Monroe, D.M. Meekhof, B.E. King, W.M. Itano, D.J. Wineland, Phys. Rev. Lett. 75 (1995) 4714.
[3] F.F. Schmidt-Kaler, H. Häffner, M. Riebe, S. Gulde, G.P.T. Lancaster, T. Deuschle, C. Becher, C.F. Roos, J. Eschner, R. Blatt, Nature 422 (2003) 408.
[4] L. Isenhower, E. Urban, X.L. Zhang, A.T. Gill, T. Henage, T.A. Johnson, T.G. Walker, M. Saffman, Phys. Rev. Lett. 104 (2010) 010503.
[5] J.L. O'Brien, G.J. Pryde, A.G. White, T.C. Ralph, D. Branning, Nature 426 (2003) 6964.
[6] T.B. Bittman, M.J. Fitch, B.C. Jacobs, J.D. Franson, Phys. Rev. A 68 (032316) (2003) 1.
[7] E. Lucero, M. Hofheinz, M. Ansmann, R.C. Bialczak, N. Katz, M. Neeley, A.D. O'Connell, H. Wang, A.N. Cleland, J.M. Martinis, Phys. Rev. Lett. 100 (2008) 247001.
[8] T. Yamamoto, Y.A. Pashkin, O. Astafiev, Y. Nakamura, J.S. Tsai, Nature 425 (2003) 941.
[9] M. Steffen, M. Ansmann, R.C. Bialczak, N. Katz, E. Lucero, R. McDermott, M. Neeley, E.M. Weig, A.N. Cleland, J.M. Martinis, Science 313 (2006) 1423.
[10] J.H. Plantenberg, P.C. de Groot, C.J.P.M. Harmans, J.E. Mooij, Nature 447 (2007) 836.
[11] L. DiCarlo, J.M. Chow, J.M. Gambetta, L.S. Bishop, B.R. Johnson, D.I. Schuster, J. Majer, A. Blais, L. Frunzio, S.M. Girvin, R.J. Schoelkopf, Nature 460 (2009) 240.
[12] Y. Makhlin, G. Schön, A. Shnirman, Rev. Mod. Phys. 73 (2001) 2.
[13] G. Wendin, V.S. Shumeiko, Low Temp. Phys. 33 (2007) 9.
[14] M.H. Devoret, A. Wallraff, J.M. Martinis, cond-mat/0411174 (2004).
[15] J.M. Martinis, Quantum Inf. Proc. 8 (2009) 81.
[16] P. Rebentrost, F.K. Wilhelm, Phys. Rev. B 79 (2009) 060507.
[17] F. Motzoi, J.M. Gambetta, P. Rebentrost, F.K. Wilhelm, Phys. Rev. Lett. 103 (2009) 110501.
[18] H. Jirari, F. Hekking, O. Buisson, Europhys. Lett. 87 (2009) 2.
[19] S. Safaei, S. Montangero, F. Taddei, R. Fazio, Phys. Rev. B 79 (2009) 064524.
[20] A.L. Pankratov, A.S. Gavrilov, Phys. Rev. B 81 (2010) 052501.
[21] S. Poletto, F. Chiarello, M.G. Castellano, J. Lisenfeld, A. Lukashenko, P. Carelli, A.V. Ustinov, Phys. Scr. T 137 (2009) 014011.
[22] A.B. Zorin, F. Chiarello, Phys. Rev. B 80 (2009) 214535.
[23] E. Hoskinson, F. Lecocq, N. Didier, A. Fay, F.W.J. Hekking, W. Guichard, O. Buisson, R. Dolata, B. Mackrodt, A.B. Zorin, Phys. Rev. Lett. 102 (2009) 097004.
[24] A.D.O'Connell, M. Hofheinz, M. Ansmann, R.C. Bialczak, M. Lenander, E. Lucero, M. Neeley, D. Sank, H. Wang, M. Weides, J. Wenner, J.M. Martinis, A.N. Cleland, Nat. doi:10.1038201008967.
[25] M. Tinkham, Introduction to Superconductivity, second ed., McGraw-Hill, New York, 1996.
[26] D.A. Jacobson, Phys. Rev. 138 (1965) 4A.
[27] T.T. Heikkilä, J. Särkkä, F.K. Wilhelm, Phys. Rev. B 66 (2002) 184513.
[28] A.A. Golubov, M.Yu. Kupriyanov, E. Il'ichev, Rev. Mod. Phys. 76 (2004) 411.
[29] N.V. Klenov, V.K. Kornev, N.F. Pedersen, Physica C 435 (2006) 114.
[30] A.M. Zagoskin, Turkish J. Phys. 27 (2003) 5.
[31] G. Wendin, V.S. Shumeiko, Superconducting quantum circuits, qubits and computing, in: M. Rieth, W. Schommers (Eds.), Handbook of Theoretical and Computational Nanotechnology, vol. 3, American Scientific, 2006.
[32] H. Zandi, A. Kokabi, A. Jafarpour, S. Khorasani, M. Fardmanesh, A. Adibi, Physica C 467 (2007) 51.
[33] S. Khorasani, B. Rashidian, J. Opt. A: Pure Appl. Opt. 4 (2002) 251.
[34] Confer to the Online Supporting Material to [9]: <http://www.sciencemag.org/cgi/content/full/313/5792/1423/DC1>.
[35] A.M. Hart, D.A. Williams, H. Ahmed, J. Phys.: Condens. Mat. 9 (1997) L197.
[36] H. Fujiki, B. Shinozaki, T. Aomine, S. Tanaka, T. Kawae, K. Takeda, Physica C 297 (1998) 309.
[37] R.W. Cohen, B. Abeles, Phys. Rev. 168 (1968) 2.
[38] K. Lin, Y.K. Kwong, M. Isaacson, J.M. Parpia, Phys. B. 165 (1990) 483.
[39] J.A. Haber, W.E. Buhro, J. Am. Chem. Soc. 120 (1998) 10847.
[40] G.R. Boogaard, A.H. Verbruggen, W. Belzig, T.M. Klapwijk, Phys. Rev. B 69 (2004) 220503.
[41] M. Steffen, J.M. Martinis, I.L. Chuang, Phys. Rev. B 68 (2003) 224518.